Journal of Material and Process Technologies

Available online at http://journal.aastu.edu.et/

Diatomite-magnetite-activated Carbon Composite: Hybrid Sorption for Lead(II) Ions from Water

Sintayehu Shewatatek[1], *Sintayehu Mekuria*[1,2], *Belete Tessema*[1,*]

[1]Department of Chemical Engineering, Addis Ababa Science and Technology University, 16417 Addis Ababa, Ethiopia
[2]Biotechnology and Bioprocess Center of Excellence, Addis Ababa Science and Technology University, 16417 Addis Ababa, Ethiopia.

Article Information

Article history:
Received 21 November 2025
Received in revised form 10 December 2025
Accepted 15 December 2025

Keywords:
Composite adsorbent
Diatomite
Teff straw
Magnetite
Lead removal

Corresponding author.
E-mail: ssmbhailu@gmail.com
https://doi.org/10.69660/jmpt.v2i1.107

Abstract

Lead (Pb (II)) contamination in aquatic systems remains a critical environmental challenge, necessitating the development of sustainable, high-efficiency adsorbents. In this study, we reported a composite material prepared from diatomite treated with sulfuric acid, teff straw-based activated carbon (TSAC), and magnetite (Fe_3O_4) to improve the removal of Pb (II) ions from aqueous solution. The adsorbent was characterized using Fourier transform infrared spectroscopy, Brunauer, Emmett and Teller, scanning electron microscope, and X-ray diffraction. At the optimum conditions (pH 7, an adsorbent dosage of 0.04 g/100 mL, an initial Pb(II) concentration of 10 mg/L, and an adsorption time of 45 min), a removal efficiency of 99.64% was achieved. The adsorption data fit best with the Sips and Freundlich isotherm models, indicating that the process involves multilayer adsorption and heterogeneous surface interactions. The composite adsorbent exhibited a maximum adsorption capacity of 144.034 mg/g, while the kinetic data were best described by the pseudo-second-order kinetic model. Thermodynamic analysis revealed that the adsorption of Pb(II) onto DE/Fe_3O_4/TSAC is spontaneous and endothermic. The adsorbent retained its adsorption efficiency over five regeneration cycles, demonstrating strong stability and reusability. These results establish DE/Fe_3O_4/TSAC as an efficient and sustainable material for Pb(II) ions removal, providing a promising solution for mitigating lead contamination in water systems.

1. Introduction

Water is vital for sustaining life and maintaining the balance of Earth's ecosystems [1]. The valuable commodity, however, has been exposed to severe threats because of the improper treatment of wastewater and increasing industrial processes, resulting in water pollution [1] . Among all the pollutants, heavy metals cause very severe and permanent harm to living organisms as well as the environment [2]. Lead is regarded as a critical environmental pollutant owing to its extensive industrial utilization and pronounced toxicity [3, 4]. Lead contamination presents serious risks to both human health and aquatic organisms, even at trace concentrations, underscoring its persistent and long-term adverse effects [4, 5].

Various technologies, including reverse osmosis, ion exchange, chemical precipitation, and membrane filtration, have been investigated for the removal of Pb(II) ions [6]. However, poses high costs, is complex, and ineffective in some cases. Among the available solutions, adsorption is a preferred choice, given its ease of operation, cost-effectiveness, and recyclability of adsorbents, thus generating minimal sludge [1, 7]. Currently, a variety of low-cost and sustainable materials, such as clays and biomass residues, are under investigation for the adsorption of Pb(II) from water [5]. Clay-based adsorbents are highly valued due to their cost-effectiveness, harmless nature, ready availability, substantial ability for cation exchange, and their surface chemistry characterized by Brønsted-Lewis acid sites [8, 9]. Diatomite is considered a promising clay-based material for heavy metal remediation owing to the abundance of surface silanol (Si–OH) groups [10], high porosity, and substantial surface area [11].

In this work, diatomite (DE)-teff straw-derived activated carbon (TSAC)-Fe_3O_4-based composite sorbent was studied for the removal of Pb(II) from water. Naturally occurring DE contains impurities of the mineral and organic compounds, which are accountable for poor wettability, fewer available reaction sites, and poor regenerations. Hence, DE was treated with H_2SO_4 before use. Activated carbon was prepared from Teff (Eragrostis tef) straw by thermal treatment after treating it with H_3PO_4.
In this study, a diatomite-teff straw-derived activated carbon-iron oxide composite sorbent was investigated for the removal of Pb(II) from water. Naturally occurring diatomite usually comprises impurities that reduce its wettability, limit available adsorption sites, and hinder regeneration performance. To overcome these limitations, diatomite was pretreated with sulfuric acid. Activated carbon was subsequently prepared from teff (Eragrostis tef) straw by thermal treatment after chemical activation with H_3PO_4. Teff is a staple cereal crop in Ethiopia, producing roughly 3 million

tonnes of straw each year [12]. Teff straw is a lignocellulosic byproduct that remains after the seeds have been harvested [13].

Teff straw-based activated carbon (TSAC) possesses distinctive characteristics, including a large surface area [14], high carbon content [15], abundant surface functional groups [16], and a stable structure [17]. It demonstrates excellent efficiency in removing both organic and inorganic pollutants, with particularly high adsorption capacity for Pb(II) ions [18]. However, activated carbon is relatively costly compared to naturally occurring clays. It can be regenerated thermally or chemically, but multiple regenerations may reduce capacity. On the other hand, natural clays such as DE can be regenerated by washing or acid treatment, resulting in lower regeneration cost. However, it shows lower heavy metal removal compared to activated carbon. Hence, a composite sorbent made from activated carbon and DE may provide optimum Pb(II) removal while incurring reasonable costs. Lately, researchers have shown growing interest in magnetic separation of spent adsorbents because it allows for effortless recovery without physically handling the adsorbent [18]. Previous studies show that the incorporation of magnetic material, such as Fe_3O_4, not only supports the separation of the sorbent from the solution but also improves the performance of the resulting adsorbent [18, 19]. This method helps the separation of adsorbents from the solution by an externally applied magnetic field, and it may also improve the adsorption capacity of the composite adsorbent [19, 20].

Clay-based magnetic composites have been investigated as novel adsorbents for the removal of heavy metals, such as Pb(II), from wastewater. Clay-based magnetic composites provide an innovative approach by allowing magnetic separation of spent adsorbents, thereby simplifying their recovery and improving overall efficiency [21, 22]. Examples of such composites include hydroxyapatite-magnetite-bentonite [23] and magnetic sepiolite/iron(III) oxide [24] composite adsorbents. To date, no studies, to the best of our knowledge, have examined the removal of Pb(II) from water using a diatomite-activated carbon-iron oxide (TDE/Fe_3O_4/TSAC) ternary composite sorbent. The TDE/Fe_3O_4/TSAC ternary composite material takes synergistic benefits primarily in the areas of adsorption and environmental remediation. The composite takes advantage of the unique property of each material: diatomite as a porous material to gain a higher surface area, magnetite for its magnetic property to ensure easy separation and recovery, and Teff straw activated carbon, which is derived from an abundant agricultural waste, for its superior ability to adsorb pollutants. Therefore, this synergy can drastically improve the efficiency of decontaminating water or other media, offering a cheap and environmentally friendly approach.

This study involved the preparation of diatomite-activated carbon-iron oxide composite adsorbent with various mass ratios from acid-treated diatomite (TDE) and teff straw activated carbon (TSAC), keeping Fe_3O_4 composition constant. The adsorbent was evaluated for its capacity to remove Pb(II) ions from aqueous solutions using batch adsorption experiments. The effects of key adsorption parameters, including initial Pb(II) ions concentration, solution pH, adsorbent dosage, and contact time, were systematically examined. Furthermore, the experimental adsorption data were fitted to adsorption isotherms and kinetic models to elucidate the adsorption mechanism. Thermodynamic calculations were also conducted to assess the feasibility of the process. Finally, a regeneration study was performed to evaluate the reusability of the adsorbent.

2. Materials and methods

2.1. Materials

Raw diatomite samples (RDE) were obtained from Adami-Tulu, Oromia regional state. Teff straw (TS) was obtained from farmland around Addis Ababa, Ethiopia. Lead nitrate (99.9%), ferric chloride hexahydrate ($FeCl_3 \cdot 6H_2O$), sodium hydroxide (98%), sulfuric acid (98%), hydrochloric acid (37%), phosphoric acid (85%), sodium chloride, acetone (99.9%), nitric acid, sodium acetate (99.5%), ethylene glycol, and 1,5-diphenylcarbazide (85%) were obtained from commercial sources. All reagents employed in this study were of analytical grade.

2.2. Adsorbent preparations

RDE was first washed with distilled water and oven-dried at 105 °C for 24 h. The dried material was then disc-milled and passed through a 69 µm sieve. The obtained sample was treated with 4 M hot H_2SO_4 for 10 h, keeping a diatomite-to-acid ratio of 50 g/L at 90 °C, with continuous stirring at 1000 rpm using a magnetic stirrer. The acid-treated diatomite (TDE) was collected by vacuum filtration and rinsed thoroughly with distilled water until a near-neutral pH was achieved. The final product was oven-dried at 105 °C for 12 h and stored in a sealed container for future use.

To prepare activated carbon from teff straw (TSAC), the straw was initially soaked overnight and then washed with water to eliminate any impurities. Then, the straw was rinsed three times using distilled water and allowed to dry in the sunlight. The straw was then ground and impregnated with 3 M H_3PO_4 for 24 h under continuous stirring. The ratio of impregnation (weight of Teff straw/weight of phosphoric acid) was 1:5674 (g/g). Following impregnation, samples were left to dry in the open air under natural sunlight and further thermal treatment was carried out at 450 °C for 2 h with a heating rate of 10 °C/min under a nitrogen flow rate of 180 cm^3/min in a muffle furnace. Following heat treatment, samples were left to cool down and washed with distilled water until the washing water pH stabilizes at the neutral pH value of 7.0. The samples were dried at 100 °C for 12 h in the oven and kept in an airtight container for further use.

To synthesize the ternary adsorbent, 1.0 g of teff straw activated carbon (TSAC) was added to 25 mL of 6 M nitric acid. The mixture was then heated under reflux for 100 min to oxidize the activated carbon [25]. The mixture was allowed to cool, after which the TSAC was washed with deionized water until the pH reached 7.0. The oxidized activated carbon was then dried in a vacuum oven at 65 °C for 24 h. To prepare the magnetic composite adsorbent, the treated diatomite (TDE) and oxidized TSAC were combined at various ratios while keeping the iron oxide concentration constant. Mixtures containing 3.0 g of iron(III) chloride hexahydrate ($FeCl_3 \cdot 6H_2O$) and 6.0 g of sodium acetate (NaAc), along with different TDE/TSAC mass ratios (0.4:1.2, 1.2:0.4, 0.8:0.8), were dispersed in 100 mL of ethylene glycol and stirred gently for 1 h. The resulting solutions were transferred into a Teflon-lined stainless-steel autoclave and subjected to thermal treatment at 200 °C for 8 h. After naturally cooling to room temperature, the samples were separated using a magnet and thoroughly washed several times with water and ethanol. Finally, the composite adsorbents were vacuum-dried at 60 °C for 24 h.

2.3. Characterizations

The surface morphology of the samples was examined using a scanning electron microscope (SEM; Inspect F50, USA) at suitable magnifications

and an accelerating voltage of 15 kV. The specific surface area of the magnetic composite adsorbent was determined via the BET (Brunauer-Emmett-Teller) method using an SA 9600 instrument. Functional groups were identified by Fourier-transform infrared (FTIR) spectroscopy (Nicolet iS50) over a wavenumber range of 4000-400 cm^{-1}. The crystallinity of the magnetite-containing composite was analyzed using X-ray diffraction (XRD-7000, Shimadzu Co., Japan) with a Cu Kα radiation source, scanning from 10° to 80°.

2.4. Adsorption experiment

2.4.1. Point of zero point of charge (pHpzc)

The acid-base titration method was employed to determine pH_{pzc} using a previously reported method [26]. Six 50 mL NaCl (0.1 M) solutions were filled in Erlenmeyer flasks and loaded with 1.0 g of the composite adsorbent. The solution pH was maintained between 2 and 12 with sodium hydroxide (0.1 M) and hydrochloric acid (0.1 M). The solutions were mixed using an orbital shaker. After 48 h, the pH of the solutions was measured, and the pH_{pzc} was determined from the point where the initial and final pH curves intersect.

2.4.2. Adsorption study

Before preparing the standard solutions, a stock solution with a concentration of 1000 ppm was prepared by dissolving 1.6146 g of Pb $(NO_3)_2$ in 1L of distilled water. Five standard solutions with concentrations of 0.2, 0.4, 0.6, 0.8, and 1 mg/L were then made by adding the $Pb(NO_3)_2$ solution to 100 mL flasks. Subsequently, each standard solution was slowly mixed with 2 mL of freshly prepared 1,5-diphenylcarbazide (1,5-DPC). Following this, 5 mL of 0.2 N H_2SO_4 was added to acidify the mixture. Each flask was carefully topped up to the calibration mark with distilled water to form the final Pb (II) solution. The concentrations of Pb (II) ions in the solutions were determined using a UV-vis spectrophotometer (UV-1800, Shimadzu) at a maximum absorption wavelength (λ max) of 500 nm, which corresponds to the characteristic absorption peak of the lead-DPC complex. The study systematically examined the effects of pH, adsorbent dosage, initial Pb (II) concentration, and contact time. Various dosages (0.025, 0.03, 0.035, 0.04, and 0.045 g) of TDE/Fe_3O_4/TSAC composite adsorbent were introduced into a 100-mL volumetric flask containing 50 mg/L of Pb (II). The mixtures were then shaken for 60 minutes at 150 rpm using an orbital shaker.

The adsorption capacity and removal efficiency were calculated using Eq. (1) and Eq. (2), respectively.

$$\text{Removal percentage } (\%) = \frac{X_o - X_f}{X_o} \text{ x } 100\% \quad (1)$$

where, X_o and X_f are the initial and final Pb (II) ion concentrations in water (mg/L), respectively.

$$\text{Adsorption capacity } (\%) = \frac{(X_i - X_f)\, x\, V}{m} x\ 100\% \quad (2)$$

where, m is the adsorbent dosage (g), and V is the volume of solution (L).

2.4.3. Adsorption kinetics, isotherms and thermodynamics

The surface interaction between adsorbate and adsorbent, and the mechanisms governing their adsorption, could be easily investigated based on various kinetic models [27]. The models examined here are the pseudo-first-order, pseudo-second-order, and intraparticle diffusion models. All the models provide information on different aspects of the adsorption process [27].

Pseudo-first order $$q_t = q_e[1 - exp^{(-K_1.t)}] \quad (3)$$

Pseudo - second order $$qt = \frac{{q_e}^2 K_2\, t}{[K_2(q_e)t+1]} \quad (4)$$

Intraparticle diffusion $$q_t = k_p t^{0.5} + c \quad (5)$$

Here, q_t (mg/g) represents the amount of Pb(II) adsorbed onto the sorbent surface at a given time t (min), while qe (mg/g) denotes the adsorption capacity of the TDE/Fe_3O_4/TSAC composite at equilibrium. The parameters k_1 and k_2 (min^{-1}) correspond to the rate constants of the pseudo-first-order and pseudo-second-order kinetic models, respectively. The intraparticle diffusion rate constant is expressed as k_p ($mg \cdot g^{-1} \cdot min^{-0.5}$), and c (mg/g) indicates the boundary layer thickness, reflecting the resistance to mass transfer.

To elucidate the adsorption mechanisms of Pb(II) on the TDE/Fe_3O_4/TSAC surface, equilibrium data were analyzed using two-parameter isotherm models (Langmuir, Freundlich, and Temkin) as well as three-parameter models (Sips and Redlich-Peterson), non-linear models.

Langmuir model (non-linear form)

Freundlich isotherm model $$q_e = K_f C_e^{\frac{1}{n}} \quad (7)$$

Temkin isotherm model $$q_e = \frac{RT}{b} (\ln K_T C_e) \quad (8)$$

Sips isotherm model $$q_e = \frac{q_{max} (K_S . C_e)^{1/n}}{1+(K_S . C_e)^{1/n}} \quad (9)$$

Redlich-Peterson isotherm model $$q_e = \frac{K_{RP} C_e}{1+ a_{RP} {C_e}^n} \quad (10)$$

In these models, q_e (mg/g) denotes the equilibrium adsorption capacity, representing the amount of Pb(II) adsorbed per unit mass of adsorbent, while C_e (mg/L) corresponds to the residual Pb(II) concentration in solution at equilibrium. The parameter q_m indicates the maximum adsorption capacity of the TDE/Fe_3O_4/TSAC composite, and K_L (L/mg) is the Langmuir constant associated with adsorption energy. For the Freundlich model, K_f and n (dimensionless) describe the adsorption capacity and adsorption intensity, respectively. In the Temkin model, b (J/mol) reflects the adsorption heat, and K_T (L/g) is the equilibrium binding constant. Temperature is expressed as T (K), and R is the universal gas constant (8.314 $J \cdot mol^{-1} \cdot K^{-1}$). For the Sips model, n_S (dimensionless) represents the heterogeneity factor, K_S (L^n/mg^n) is the Sips constant, and a_{R-P} (L/g) is the Redlich-Peterson constant. These parameters were obtained through non-linear regression fitting of the isotherm models.

Adsorption thermodynamics examines how temperature influences the interaction between adsorbents and adsorbates during sorption processes. Assessing the spontaneity of an adsorption reaction requires analysing key thermodynamic parameters [28]. These parameters include the Gibbs free energy change (ΔG^o), enthalpy change (ΔH^o), entropy change (ΔS^o), and activation energy (E_a), which are determined from batch sorption experiments conducted at different temperatures and contact times [29]. The Gibbs free energy change (ΔG^o) is a key parameter for evaluating the thermodynamic feasibility of the process. A negative ΔG^o value indicates that the sorption occurs spontaneously and is energetically favourable. This parameter is typically calculated from the equilibrium constant, as shown in Equation (11) [29].

$$\Delta G^o = -RTln(K) \quad (11)$$

Here, K_c denotes the equilibrium constant, and T represents the absolute temperature in Kelvin (K).

Enthalpy change (ΔH^o) refers to the heat exchanged under constant pressure conditions without non-expansion work [28]. It is typically measured experimentally via calorimetry by observing temperature changes during adsorption. The Van't Hoff equation (Equation (12) establishes the thermodynamic relationship to calculate ΔH^o for adsorption systems. A negative ΔH^o indicates that the adsorption process is exothermic, whereas a positive ΔH^o signifies an endothermic reaction.

$$logK_C = \frac{\Delta S^o}{2.303R} = \frac{\Delta H}{2.303RT} \quad (12)$$

Here, KC is the dimensionless distribution coefficient, as defined in Equation (13).

$$K_C = \frac{C_{ad}}{C_e} \quad (13)$$

Here, Cad represents the amount of metal ions adsorbed at equilibrium (mg/L), and Ce denotes the concentration of the solute remaining in the solution (mg/L).

The entropy change (ΔS^o) reflects the level of disorder or randomness within a system during adsorption. It is determined from the slope of the linear Van't Hoff plot (log K_C versus 1/T), as described in Equation (12). A positive ΔS^o indicates an increase in disorder at the adsorbent-adsorbate interface, suggesting a strong affinity between the adsorbent and the adsorbate [29]. Here, K_2 is the rate constant of pseudo-second order, and K_0 is the Arrhenius constant.

2.4.4. Regeneration test

The reusability of the adsorbent was evaluated through consecutive adsorption-desorption cycles. Pb(II) ions were first adsorbed from 100 mL of a 50 mg/L solution. After reaching adsorption equilibrium, the adsorbent was separated using a bar magnet. The recovered TDE/Fe_3O_4/TSAC composite was then dried and immersed in 50 mL of 0.2 N HCl, followed by agitation for 2 h to desorb the metals and regenerate the pores [30]. The suspension was stirred at 150 rpm for 45 min. Subsequently, the adsorbent was washed with deionized water, isolated, dried at 65 °C, and reused in the next adsorption cycle.

3. Results and discussion

3.1. Characterizations

Figure 1 indicates FTIR, XRD, SEM and pH_{pzc} of the TDE/Fe_3O_4/TSAC composite adsorbent. As shown in Figure 1(a), the FTIR spectra reveal a Fe-O stretching vibration at 553.89 cm^{-1} [31, 32], while the peaks at 3,331 and 1,640 cm^{-1} correspond to the O-H stretching vibrations of the silanol groups in the diatomite [33]. The absorption at 803.54 cm^{-1} is attributed to Si-O stretching in the silica shell [31]. The peak at 1,066 cm^{-1} arises from C-O stretching of the carbonyl groups present in the composite [34], and the band at 2,107.19 cm^{-1} may be associated with C-H stretching vibrations [14].

The crystal structure of the magnetic composite adsorbent was analyzed using XRD (Figure 1(b)). Diffraction peaks at 2θ = 30.5°, 35.28°, 42.5°, and 63.16° correspond to the characteristic patterns of Fe_3O_4, confirming the presence of crystalline Fe_3O_4 particles in the composite [35, 36]. A weak peak at 2θ = 26.6° is attributed to activated carbon [37], while additional weak peaks at low angles indicate the amorphous nature of SiO_2 [33]. These results confirm the successful synthesis of the magnetic TDE/Fe_3O_4/TSAC composite adsorbent.

Figure 1(c) shows the SEM image of the TDE/Fe_3O_4/TSAC composite adsorbent, revealing a heterogeneous and irregular surface with a combination of spherical, elliptical, and rod-like structures. The spherical morphology arises from the Fe_3O_4 nanoparticles, while the diatomite contributes the elliptical and rod-like features, in agreement with previous reports [38]. Many of the spherical particles form agglomerates with asymmetric distribution, characteristic of iron oxide nanoparticles. The synthesized composite exhibits a high BET surface area of 347.458 m^2/g, reflecting its porous and well-developed surface architecture.

The point of zero charge (pH_{pzc}) of the TDE/Fe_3O_4/TSAC surface was determined to be pH 5 (Figure 1(d)). At pH values above 5, the surface carries a negative charge, enhancing electrostatic attraction toward positively charged Pb(II) ions and thereby increasing removal efficiency [39]. Conversely, at pH values below the pH_pzc, the surface becomes protonated, resulting in electrostatic repulsion with Pb(II) ions and reduced adsorption efficiency.

3.2. Adsorption studies

Adsorption studies were conducted on TDE/Fe_3O_4/TSAC composites that were synthesized with different mixing ratios (1.2/0.4, 0.4/1.2, and 0.8/0.8) of TSAC to DE (w/w), and the results are presented in Figure 2. The Fe_2O_3 content was kept constant. The TSAC-to-TDE ratio significantly influenced the Pb (II) removal percentage and the subsequent surface area of the adsorbent.

Composite with TSAC/TDE ratio of 1.2: 0.4 showed 95.48 % Pb(II) ions removal percentage and a BET specific surface area of 331.44 m2/g. On the other hand, adsorbent with TSAC/TDE ratio 0.4:1.2 resulted in a lower removal efficiency of 87.25 % and a lower surface area of 173.187 m2/g. A maximum removal efficiency 99.56 % was achieved with a composite adsorbent with TSAC/DE ratio of 0.8:0.8, which shows a higher BET surface area of 347.458 m^2/g. For this adsorbent, the effect of pH of solution, adsorption dosage, adsorption time, and initial lead concentration was further investigated.

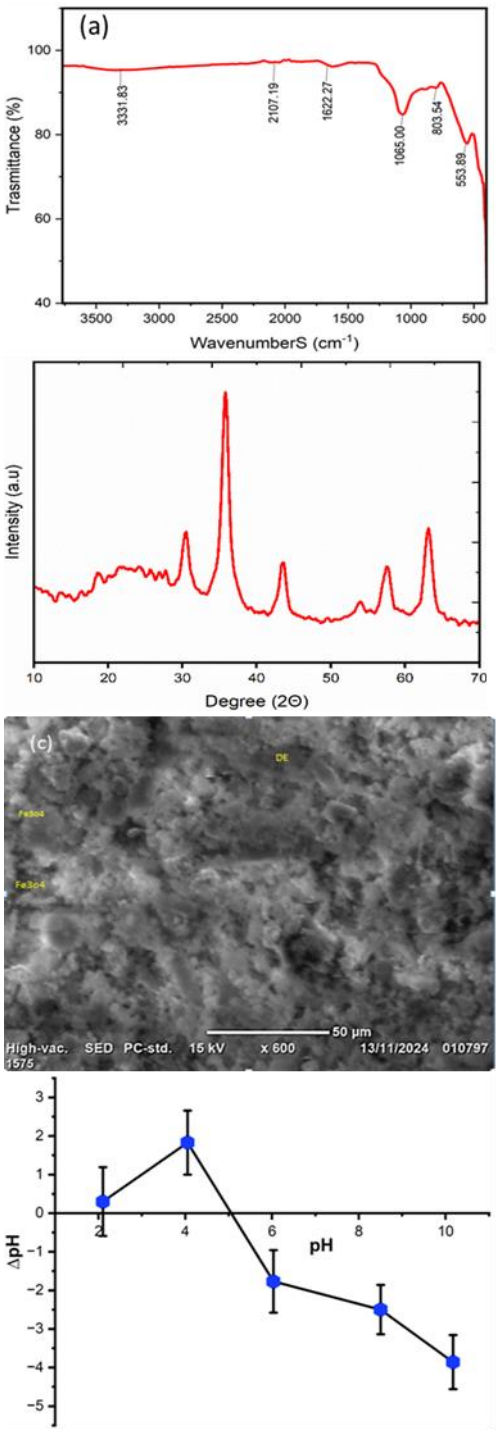

Figure 1. Characterization of TDE/Fe_3O_4/TSAC composite: (a) FTIR spectrum, (b) XRD pattern, (c) SEM micrograph, and (d) point of zero charge (pH_pzc) graph.

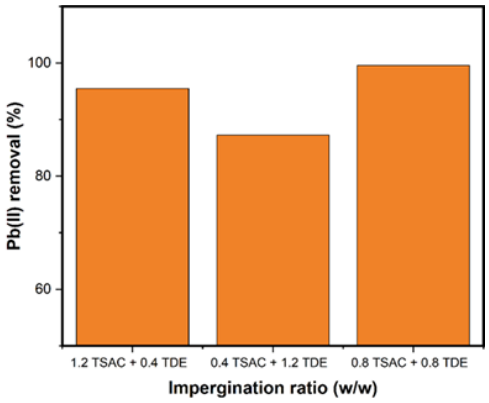

Figure 2. Influence of the activated carbon-to-diatomite ratio on Pb(II) removal by TDE/Fe_3O_4/TSAC.

3.2.1. Adsorption parameters effect

Figure 3 shows the effects of adsorbent dosage, adsorption time, solution pH and initial Pb(II) ions concentration on percentage removal. The effect of TDE/Fe_3O_4/TSAC dosage on Pb(II) removal efficiency was evaluated at 0.025, 0.03, 0.035, 0.04, and 0.045 g per 100 mL of solution. The Pb(II) ions removal percentage shows 81.55 %, 88.78 %, 92.86 %, 96.87 %, and 97.259 % for adsorbent dosage of 0.025, 0.03, 0.035, 0.04, and 0.045 g, respectively (Figure 3 (a)). The removal efficiency of the composite increased significantly with adsorbent dosage up to 0.04 g, beyond which it plateaued, indicating surface saturation. At this point, most active sites on the adsorbent are occupied by Pb(II) ions, and further increases in dosage have minimal effect on adsorption. This behaviour reflects the interplay between the adsorbent's surface area and the lead ion concentration, where adsorption slows as saturation is approached. Understanding this saturation point is essential for optimizing adsorbent use and achieving cost-effective Pb(II) removal.

The effect of contact time on Pb(II) removal by the TDE/Fe_3O_4/TSAC composite was investigated over 15-75 min. Adsorption was initially rapid due to the abundance of available active sites (Figure 3(b)), but gradually slowed as the sites became occupied and the heterogeneous surface structure limited further uptake [40]. At 45 min, the removal efficiency reached 96.75%, as extended contact allowed Pb(II) ions a greater opportunity to diffuse and interact with the adsorbent surface [40].

Batch experiments were performed at pH 2-10 to examine its effect on Pb(II) removal (Figure 3(c)). Pb(II) uptake increased with pH, peaking at pH 7, due to the negatively charged surface of TDE/Fe_3O_4/TSAC enhancing electrostatic attraction with the positively charged ions. At lower pH, hydrogen ions compete with Pb(II) for active sites, reducing adsorption, while at pH above 7, Pb(II) precipitates as $Pb(OH)_2$, which cannot be adsorbed [41]. As initial Pb (II) concentration increases from 10 to 50 mg/L, the adsorption efficiency of the DE/Fe_3O_4/TSAC composite initially reduced from 99.64 % to 93.69 %, as shown in Figure 3 (d). The efficiency of Pb (II) adsorption on TDE/Fe_3O_4/TSAC initially shows great performance, mechanistically due to the high density of available active sites on the composite surface [42], which shows a strong affinity towards the contaminant. However, with increasing Pb(II) concentrations, the Pb(II)

ions removal capacity decreases [43] largely due to two synergistic effects: (i) site saturation, because persistent occupation of surface-active sites reduces available binding sites, and (ii) inter-adsorbate interference, because higher ionic densities result in competitive adsorbate species interactions that destroy adsorption equilibria through steric hindrance and electrostatic repulsion effects.

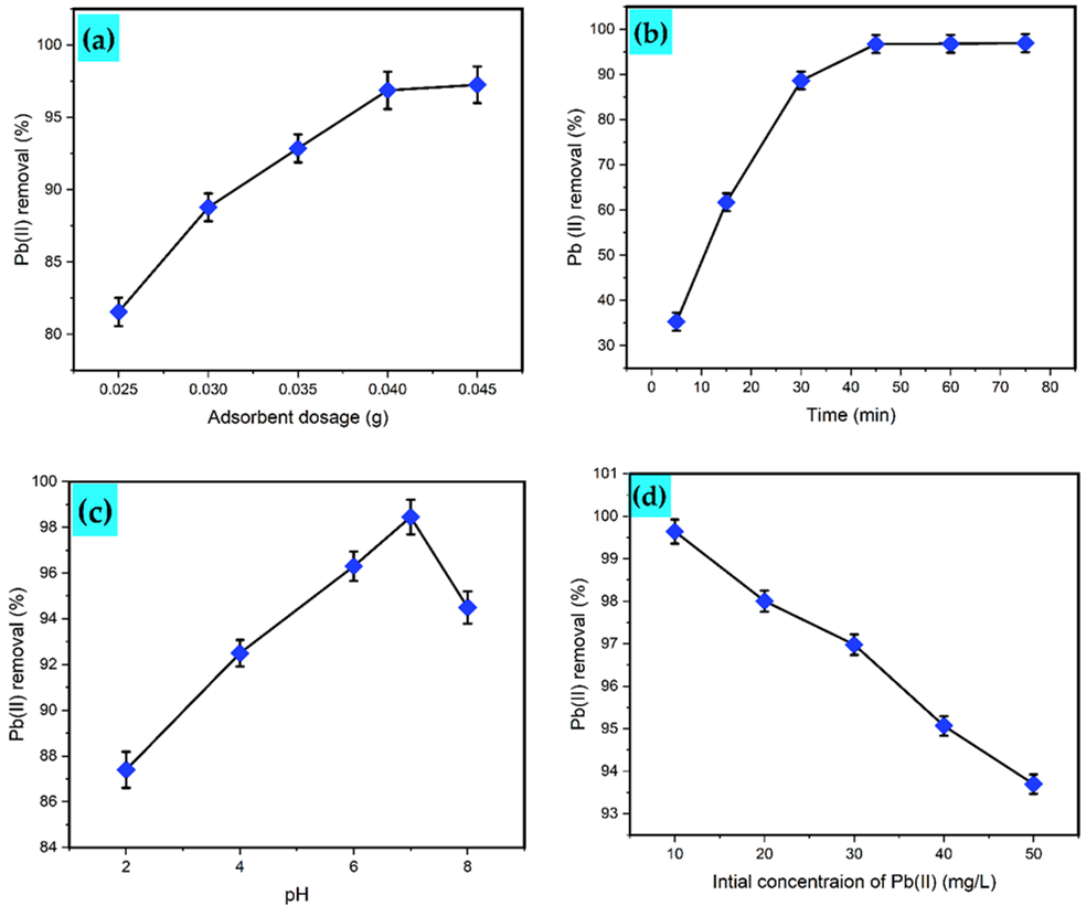

Figure 3. Effect of adsorption parameters on Pb(II) removal efficiency: (a) adsorbent dosage, (b) contact time, (c) solution pH, and (d) initial Pb(II) concentration.

Table 1. Pb(II) isotherm parameters for DE/Fe_3O_4/TSAC.

Model	Equation	Parameters			Statistical indices			
Langmuir's Isotherm	$q_e = \frac{q_m K_L C_e}{1 + K_L C_e}$	q_m (mg/g)	K_L (L/mg)		R^2	Δq	χ^2	ARE
		137.87	1.351		0.9228	3.023	0.734	0.152
Freundlich's isotherm	$q_e = K_f C_e^{\frac{1}{n}}$	K_f (L/g)	n		R^2	Δq	χ^2	ARE
		74.54	2.62		0.99365	2.265	0.625	0.134
Temkin's isotherm	$q_e = \frac{RT}{b} (\ln K_T C_e)$	K_T (L/g)	b (J/mol)		R^2	Δq	χ^2	ARE
		1.3123	2.607		0.9053	7.975	2.46	1.001
Sips's isotherm	$q_e = \frac{q_m (K_S C_e)^{1/n}}{1 + (K_S C_e)^{1/n}}$	q_m (mg/g)	n	K_s (L/g)	R^2	Δq	χ^2	ARE
		144.034	0.579	1.611	0.99363	2.43	0.397	0.079
Redlich- Peterson's isotherm	$q_e = \frac{K_{RP} C_e}{1 + a_{RP} C_e^{\,n}}$	K_{RP} (L/g)	n	a_{RP} (L^n/mg^{-n})	R^2	Δq	χ^2	ARE
		1.7736	0.618	2.379	0.99365	2.233	0.391	0.061
Tóth's isotherm	$q_e = \frac{q_{\max} K_T C_e}{[1 + (K_T C_e)^n]^{1/n}}$	K_T (mg/L)	n	q_{max} (mg/g)	R^2	Δq	χ^2	ARE
		4.401	0.0245	143.15	0.99256	2.83	0.219	0.050

Journal of Material and Process Technologies

Available online at http://journal.aastu.edu.et/

3.2.2. Adsorption isotherm study

Equilibrium adsorption data were analyzed using the Langmuir, Freundlich, Temkin, and three-parameter isotherm models to investigate the adsorption mechanism and determine the maximum adsorption capacity of the DE/Fe_3O_4/TSAC composite (Figure 4 and Table 1). Pb(II) isotherm experiments were conducted under optimal conditions: 100 mL solution, 150 rpm agitation, pH 7, 45 min contact time, 25 °C, and 0.04 g adsorbent, with initial Pb(II) concentrations ranging from 10 to 50 mg/L. The best-fitting isotherm was identified by comparing the coefficients of determination (R^2), providing insight into the adsorption mechanism.

Three-parameter isotherms (Sips, Tóth, Redlich–Peterson) fit the data exceptionally well ($R^2 > 0.9925$, ARE ≤ 0.050%), indicating a heterogeneous multilayer adsorption mechanism. The Redlich–Peterson and Freundlich models ($R^2 = 0.9937$ and 0.9228, respectively) confirm multilayer adsorption on a moderately heterogeneous surface, while the less satisfactory fits of Temkin ($R^2 = 0.9053$) and Langmuir ($R^2 = 0.9228$) suggest limited monolayer contribution. Overall, the adsorption is best described as a hybrid mechanism combining multilayer coverage and surface heterogeneity.

Table 2 shows constant parameters for the adsorption kinetics.

Model	Equations	Parameter		Statistical indices			
PFO	$q_t = q_{e1}\,[1 - exp^{(-k_1.t)}]$	q_{e1} (mg/g)	k_1 (1/min)	R^2	Δq	χ^2	ARE
		121.93	0.075	0.9861	5.3	1.45	0.60
PSO	$q_t = \frac{{q_{e2}}^2 k_2 t}{[k_2\, q_{e2}\, t + 1]}$	q_{e2} (mg/g)	k_2 (g/mg min)	R^2	Δq	χ^2	ARE
		144.44	6.084	0.989	2.69	0.29	0.12

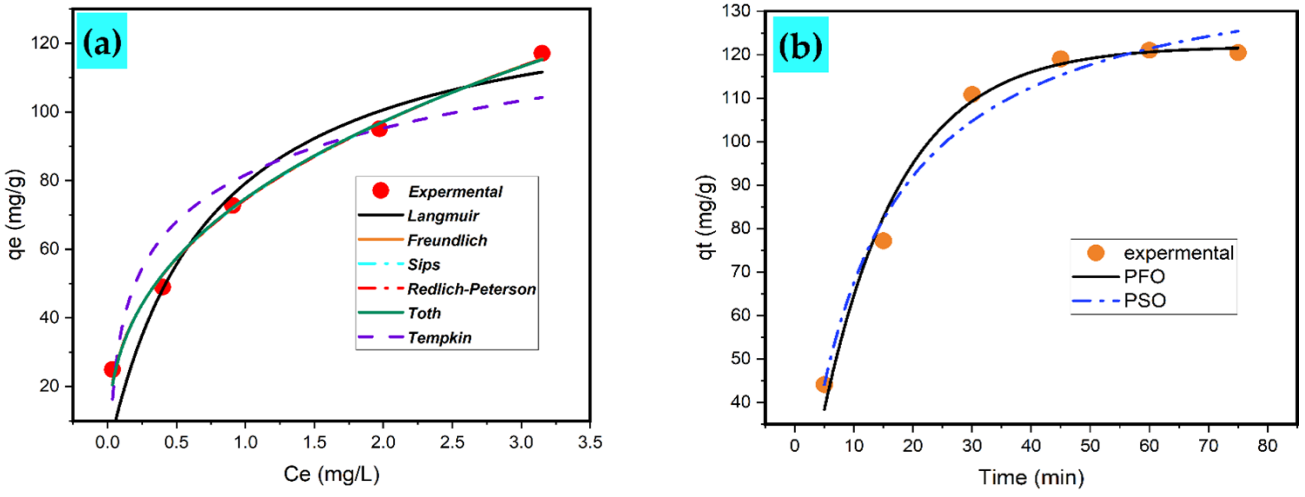

Figure 4. Isotherm and mad kinetics models. (a) isotherm models, (b) kinetics models.

Table 3. Thermodynamic parameters for Pb(II) adsorption onto TDE/Fe_3O_4/TSAC, derived from plotting ln Kc versus 1/T.

Temperature (K)	K_L	ΔG^0 (kJ/mol)	ΔH^0 (kJ/mol)	ΔS^0 (J/mol)
303	27.022	-8.12497	39.65493	178.96
308	29.303	-8.46199		
313	30.9557	-8.73898		
318	33.0754	-9.04983		
323	43.9599	-9.93946		

3.2.3. Adsorption kinetics study

Batch experiments were conducted using 100 mL of aqueous solutions containing an initial Pb(II) concentration of 10.0 mg/L and 0.04 g of DE/Fe_3O_4/TSAC at pH 7 and 25 °C to systematically investigate sorption kinetics. The rate-limiting processes were analyzed using two mechanistic models: pseudo-first-order (PFO) and pseudo-second-order (PSO). Kinetic results showed a better fit with the PSO model (R^2 > 0.98), yielding an equilibrium adsorption capacity (q_e) of 144.44 mg/g. This strong correlation suggests chemisorption as the dominant mechanism, likely involving covalent electron transfer between the active surface sites on DE/Fe_3O_4/TSAC and Pb(II) ions, consistent with observations reported in the literature [44].

3.2.4. Thermodynamics

Batch adsorption of Pb(II) onto TDE/Fe_3O_4/TSAC was evaluated at 303–323 K with an initial metal concentration of 50 mg/L, adsorbent dosage of 0.04 g/100 mL, pH 7, and 150 rpm agitation for 45 min. Thermodynamic analysis revealed negative ΔG^o values across all temperatures, confirming the spontaneity of the process. Van't Hoff analysis (ln KL vs. 1/T) yielded ΔH^o = 39.65 kJ/mol and ΔS^o = 178.96 J/(mol·K), indicating an endothermic adsorption accompanied by increased molecular disorder at the solid-liquid interface. The minimal variation in ΔG^o with temperature further supports the endothermic and thermodynamically favorable nature of Pb(II) uptake by TDE/Fe_3O_4/TSAC. Table 3 shows the thermodynamic parameters for the adsorption process, and Figure 5 shows a plot of ln Kc versus 1/T.

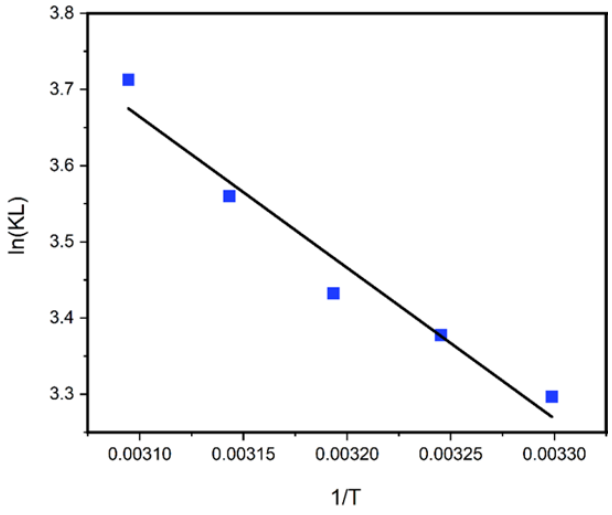

Figure 5. Adsorption data plotted as ln Kc versus 1/T.

3.2.5. Regeneration test

The reusability of TDE/Fe_3O_4/TSAC and the safe disposal of treated wastewater are critical for assessing its economic viability. Figure 6 shows the adsorbent's performance over five consecutive cycles, with Pb (II) removal efficiencies of 94.3%, 92.7%, 91.3%, 88.5%, and 85.0%, respectively. It shows a total decline of only 9.8% in the five cycles. These results demonstrate that TDE/Fe_3O_4/TSAC maintains its adsorption capacity and structural integrity after regeneration, confirming robust reusability. The slight decrease in efficiency may be attributed to pore blockage by adsorbed contaminants, as indicated by pseudo-second-order kinetics. Overall, this composite remains a highly effective and cost-efficient adsorbent for practical Pb(II) removal applications.

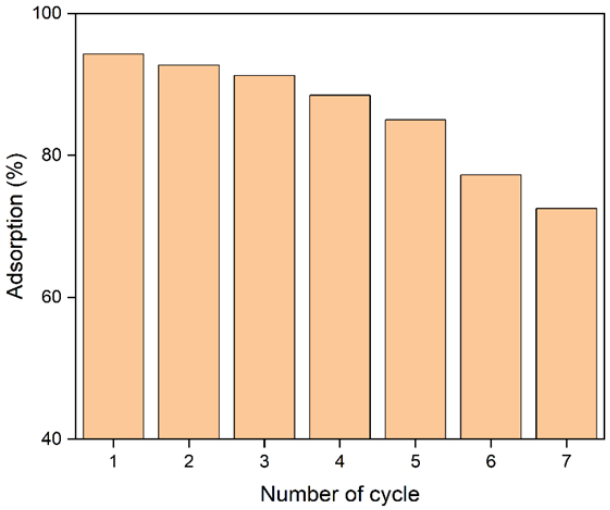

Figure 6. Performance of DE/Fe_3O_4/TSAC composite in Pb(II) removal over five consecutive adsorption–desorption cycles.

3.2.6. Mechanism of Pb(II) sorption

The DE/Fe_3O_4/TSAC composite, synthesized from sulfuric acid-treated diatomite, teff straw activated carbon (TSAC), and magnetite, exploits synergistic interactions for efficient Pb^{2+} removal from aqueous solutions [44]. Sulfuric acid treatment enhances diatomite's porosity and introduces sulfate ($SO_4$2-) and silanol (-Si-OH) groups, promoting ion exchange and complexation with Pb (II) [45, 46]. TSAC provides high surface area and oxygenated functional groups (-COOH, -OH) that enable adsorption via electrostatic attraction and surface complexation [47]. Magnetite (Fe_3O_4) facilitates magnetic recovery and offers Fe–O sites for Pb^{2+} coordination.

The composite's hierarchical pore structure, that is, macropores diatomite and micropores from TSAC enhances Pb (II) diffusion and accessibility to active sites, while dispersed magnetite nanoparticles prevent aggregation and improve adsorption capacity [48]. Multifunctional sites (sulfate, carboxyl, hydroxyl) enable ion exchange, surface complexation, and electrostatic binding. BET and FTIR analyses confirm enhanced porosity, active functional group participation, and Pb^{2+} binding mechanisms. Adsorption follows Freundlich and Redlich–Peterson isotherms (multilayer coverage) and pseudo-second-order kinetics, indicating chemisorption dominance. Optimal removal occurs at pH 6-8, balancing electrostatic attraction and preventing $Pb(OH)_2$ precipitation. The composite demonstrates reusability with acid regeneration restoring active sites, combining high adsorption capacity, structural stability, and practical recoverability. Compared to its individual components and other composites, this material offers cost-effective, sustainable, and efficient heavy metal remediation, leveraging agricultural waste and natural diatomite for wastewater applications.

4. Conclusions

The DE/Fe_3O_4/TSAC composite, synthesized from sulfuric acid-treated diatomite, teff straw activated carbon (TSAC), and magnetite, demonstrated excellent efficiency for Pb (II) removal due to synergistic physicochemical interactions among its components. Optimization of the TSAC-to-TDE ratio and detailed characterization (FTIR, SEM, XRD, BET) revealed a microporous structure with a high surface area (347.45 m^2/g) and abundant active sites, while the point of zero charge indicated favourable surface charge properties for adsorption at pH greater than 5. Under optimized conditions (pH 7, adsorbent dosage 0.04 g/100 mL, initial Pb (II) concentration 10 mg/L, and 45 min contact time), the composite achieved a maximum Pb (II) removal efficiency of 99.64% and an adsorption capacity of 144.03 mg/g. Adsorption followed Freundlich, Langmuir, and Toth isotherms, suggesting multilayer coverage and heterogeneous surface interactions, while pseudo-second-order kinetics confirmed chemisorption as the rate-limiting step. Thermodynamic analysis indicated spontaneous and endothermic adsorption. The composite exhibited excellent reusability, maintaining high efficiencies over five consecutive cycles (from 94.3% to 85.0%), highlighting its structural stability and practical applicability. However, these results were obtained under controlled laboratory conditions; future studies should address long-term stability, the influence of co-existing ions, and real wastewater matrices. Overall, the DE/Fe_3O_4/TSAC composite represents a cost-effective, sustainable, and high-performance adsorbent for heavy metal remediation, combining high adsorption capacity, structural robustness, and potential for practical wastewater treatment applications.

Declaration of competing interest

The authors declare that they have no competing interests.

Acknowledgments

The authors gratefully acknowledge Addis Ababa Science and Technology (AASTU).

References

[1] P. Zhang, M. Yang, J. Lan, Y. Huang, J. Zhang, S. Huang, Y. Yang, J. Ru, Water quality degradation due to heavy metal contamination: health impacts and eco-friendly approaches for heavy metal remediation, Toxics 11(10) (2023) 828.

[2] K.H. Vardhan, P.S. Kumar, R.C. Panda, A review on heavy metal pollution, toxicity and remedial measures: Current trends and future perspectives, Journal of Molecular Liquids 290 (2019) 111197.

[3] P. Jarvis, J. Fawell, Lead in drinking water–an ongoing public health concern?, Current Opinion in Environmental Science & Health 20 (2021) 100239.

[4] A.L. Obsa, N.T. Shibeshi, E. Mulugeta, G.A. Workeneh, Bentonite/amino-functionalized cellulose composite as effective adsorbent for removal of lead: Kinetic and isotherm studies, Results in Engineering 21 (2024) 101756.

[5] I.R. Chowdhury, S. Chowdhury, M.A.J. Mazumder, A. Al-Ahmed, Removal of lead ions (Pb2+) from water and wastewater: a review on the low-cost adsorbents, Applied Water Science 12(8) (2022) 185.

[6] M.A. Aziz, I.R. Chowdhury, M.A.J. Mazumder, S. Chowdhury, Highly porous carboxylated activated carbon from jute stick for removal of Pb 2+ from aqueous solution, Environmental Science and Pollution Research 26 (2019) 22656-22669.

[7] S. Maleki, A. Karimi-Jashni, Optimization of Ni (II) adsorption onto Cloisite Na+ clay using response surface methodology, Chemosphere 246 (2020) 125710.

[8] E. Padilla-Ortega, N. Medellín-Castillo, A. Robledo-Cabrera, Comparative study of the effect of structural arrangement of clays in the thermal activation: Evaluation of their adsorption capacity to remove Cd (II), Journal of Environmental Chemical Engineering 8(4) (2020) 103850.

[9] I. Kovalchuk, Clay-based sorbents for environmental protection from inorganic pollutants, Environmental Sciences Proceedings 25(1) (2023) 34.

[10] H. Mohamedbakr, M. Burkitbaev, Elaboration and characterization of natural diatomite in Aktyubinsk/Kazakhstan, The Open Mineralogy Journal 3(1) (2009) 12-16.

[11] N.A. Fathy, S.M. Mousa, R.M. Aboelenin, M.A. Sherief, A.S. Abdelmoaty, Strengthening the surface and adsorption properties of diatomite for removal of Cr (VI) and methylene blue dye, Arabian Journal of Geosciences 15(22) (2022) 1664.

[12] W.A. Woldie, N.T. Shibeshi, K.D. Kuffi, Optimization of cellulose nanocrystals extraction from teff straw using acid hydrolysis followed by ultrasound sonication, Carbohydrate Polymer Technologies and Applications 9 (2025) 100707. https://doi.org/https://doi.org/10.1016/j.carpta.2025.100707.

[13] N.C. Corda, M.S. Kini, A review on adsorption of cationic dyes using activated carbon, MATEC web of conferences, EDP Sciences, 2018, p. 02022.

[14] S. Shewatatek, G. Gonfa, S. Mekuria, B. Tessema, Response Surface Optimization of Lead Adsorption onto Teff Straw-Derived Activated Carbon, Results in Surfaces and Interfaces (2024) 100378.

[15] S.M. Beyan, S.V. Prabhu, T.A. Ambio, C. Gomadurai, A statistical modeling and optimization for Cr (VI) adsorption from aqueous media via teff straw-based activated carbon: isotherm, kinetics, and thermodynamic studies, Adsorption Science & Technology 2022 (2022) 7998069.

[16] K. Siraj, J.S. Aballa, M. Danish, T. Ahmad, M.M. Khan, S. Majeed, B. Adane, The effect of microwave and muffle furnace-assisted heating on the surface characteristics of teff husk activated carbons: Thermodynamic, isotherm, and kinetics study of Pb removal, Diamond and Related Materials 143 (2024) 110912.

[17] T.A. Amibo, S.M. Beyan, T.M. Damite, Novel lanthanum doped magnetic teff straw biochar nanocomposite and optimization its efficacy of defluoridation of groundwater using RSM: a case study of hawassa city, Ethiopia, Advances in Materials Science and Engineering 2021(1) (2021) 9444577.

[18] S. Moosavi, C.W. Lai, S. Gan, G. Zamiri, O. Akbarzadeh Pivehzhani, M.R. Johan, Application of efficient magnetic particles and activated carbon for dye removal from wastewater, ACS omega 5(33) (2020) 20684-20697.

[19] İ. Alacabey, Endosulfan elimination using amine-modified

magnetic diatomite as an adsorbent, Frontiers in chemistry 10 (2022) 907302.
[20] X. Liu, H. Liu, K. Cui, Z. Dai, B. Wang, R. Weerasooriya, X. Chen, Adsorption-reduction of Cr (VI) with magnetic Fe-CN composites, Water 15(12) (2023) 2290.
[21] N. Wahab, M. Saeed, M. Ibrahim, A. Munir, M. Saleem, M. Zahra, A. Waseem, Synthesis, characterization, and applications of silk/bentonite clay composite for heavy metal removal from aqueous solution, Frontiers in chemistry 7 (2019) 654.
[22] Z. Baimuratova, S. Ermekov, A. Silva, H. Gomes, M. Kalmakhanova, New magnetic clays MnFe2O4/Shymkent for removal of heavy metals from wastewater, E3S Web of Conferences, EDP Sciences, 2024, p. 01034.
[23] Q.U. Ain, H. Zhang, M. Yaseen, U. Rasheed, K. Liu, S. Subhan, Z. Tong, Facile fabrication of hydroxyapatite-magnetite-bentonite composite for efficient adsorption of Pb (II), Cd (II), and crystal violet from aqueous solution, Journal of Cleaner Production 247 (2020) 119088.
[24] O. Uygun, A. Murat, G.Ö. Çakal, Magnetic sepiolite/iron (III) oxide composite for the adsorption of lead (II) ions from aqueous solutions, Clay Minerals 58(3) (2023) 267-279.
[25] X. Shan, S. Tan, Y. Shi, J. Shao, K. Su, L. Zhang, H. Feng, H. Ye, Activated carbon/diatomite-based magnetic nanocomposites for magnetic solid-phase extraction of S-phenylmercapturic acid from human urine, Biomedical Chromatography 34(7) (2020) e4834.
[26] T. Anirudhan, M. Ramachandran, Adsorptive removal of basic dyes from aqueous solutions by surfactant modified bentonite clay (organoclay): kinetic and competitive adsorption isotherm, Process Safety and Environmental Protection 95 (2015) 215-225.
[27] T.L. Tan, H. Nakajima, S.A. Rashid, Adsorptive, kinetics and regeneration studies of fluoride removal from water using zirconium-based metal organic frameworks, RSC advances 10(32) (2020) 18740-18752.
[28] P. Saha, S. Chowdhury, Insight into adsorption thermodynamics, Thermodynamics 16 (2011) 349-364.
[29] A.N. Ebelegi, N. Ayawei, D. Wankasi, Interpretation of adsorption thermodynamics and kinetics, Open Journal of Physical Chemistry 10(3) (2020) 166-182.
[30] A. Jafari Kang, M. Baghdadi, A. Pardakhti, Removal of cadmium and lead from aqueous solutions by magnetic acid-treated activated carbon nanocomposite, Desalination and Water Treatment 57(40) (2016) 18782-18798.
[31] H.-m. Jiang, Z.-p. Yan, Y. Zhao, X. Hu, H.-z. Lian, Zincon-immobilized silica-coated magnetic Fe3O4 nanoparticles for solid-phase extraction and determination of trace lead in natural and drinking waters by graphite furnace atomic absorption spectrometry, Talanta 94 (2012) 251-256.
[32] Z. Zhang, J. Kong, Novel magnetic Fe3O4@ C nanoparticles as adsorbents for removal of organic dyes from aqueous solution, Journal of hazardous materials 193 (2011) 325-329.
[33] Y.-P. Chang, C.-L. Ren, Q. Yang, Z.-Y. Zhang, L.-J. Dong, X.-G. Chen, D.-S. Xue, Preparation and characterization of hexadecyl functionalized magnetic silica nanoparticles and its application in Rhodamine 6G removal, Applied Surface Science 257(20) (2011) 8610-8616.
[34] D. Mohan, A. Sarswat, V.K. Singh, M. Alexandre-Franco, C.U. Pittman Jr, Development of magnetic activated carbon from almond shells for trinitrophenol removal from water, Chemical Engineering Journal 172(2-3) (2011) 1111-1125.
[35] J. Wang, S. Zheng, Y. Shao, J. Liu, Z. Xu, D. Zhu, Amino-functionalized Fe3O4@ SiO2 core–shell magnetic nanomaterial as a novel adsorbent for aqueous heavy metals removal, Journal of colloid and interface science 349(1) (2010) 293-299.
[36] A. Donia, A. Atia, F. Abouzayed, Preparation and characterization of nano-magnetic cellulose with fast kinetic properties towards the adsorption of some metal ions, Chemical Engineering Journal 191 (2012) 22-30.
[37] V. Ranjithkumar, A.N. Hazeen, M. Thamilselvan, S. Vairam, Magnetic activated carbon-Fe3O4 nanocomposites—synthesis and applications in the removal of acid yellow dye 17 from water, Journal of nanoscience and nanotechnology 14(7) (2014) 4949-4959.
[38] Z. Akbari-Jonoush, S. Naseri, M. Farzadkia, H.-R. Mohajerani, M. Shirzad-Siboni, J.-K. Yang, Application of C14/SiO2–Fe3O4 and AC–Fe3O4 nanocomposite for U (VI) removal, Desalination and Water Treatment 57(47) (2016) 22519-22532.
[39] M. Kosmulski, The pH dependent surface charging and points of zero charge. IX. Update, Advances in Colloid and Interface Science 296 (2021) 102519.
[40] R. Foroutan, S.J. Peighambardoust, R. Mohammadi, M. Omidvar, G.A. Sorial, B. Ramavandi, Influence of chitosan and magnetic iron nanoparticles on chromium adsorption behavior of natural clay: adaptive neuro-fuzzy inference modeling, International journal of biological macromolecules 151 (2020) 355-365.
[41] Y. Li, T. Ran, H. Yang, Z. Dong, Y. Shi, Ir-reversible on/off switching hydrogel for efficient dye capture and release, Journal of Environmental Chemical Engineering 11(3) (2023) 109829.
[42] J. Fito, M. Abewaa, T. Nkambule, Magnetite-impregnated biochar of parthenium hysterophorus for adsorption of Cr (VI) from tannery industrial wastewater, Applied Water Science 13(3) (2023) 78.
[43] K. Brungesh, B. Nagabhushana, M. Harish, R. Hari Krishna, An efficient removal of toxic Cr (VI) from aqueous solution by MnO2 coated polyaniline nanofibers: kinetic and thermodynamic study, J. Environ. Anal. Toxicol 7(2161) (2017) 2161-0525.1000442.
[44] Z. Deng, S. Gu, H. Cheng, D. Xing, G. Twagirayezu, X. Wang, W. Ning, M. Mao, Removal of phosphate from aqueous solution by zeolite-biochar composite: adsorption performance and regulation mechanism, Applied Sciences 12(11) (2022) 5334.